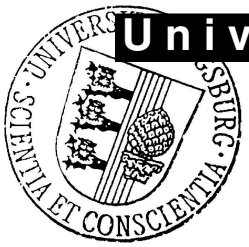

Universität Augsburg

Institut für Mathematik

Harbir Antil, Ronald H.W. Hoppe, Christopher Linsenmann

Optimal Design of Stationary Flow Problems by Path-Following Interior-Point Methods

Preprint Nr. 002/2007 — 22. Mai 2007

Institut für Mathematik, Universitätsstraße, D-86 135 Augsburg http://www.math.uni-augsburg.de/

Impressum:

Herausgeber:

Institut für Mathematik
Universität Augsburg
86135 Augsburg
http://www.math.uni-augsburg.de/forschung/preprint/

ViSdP:

Ronald H.W. Hoppe
Institut für Mathematik
Universität Augsburg
86135 Augsburg

Structural and Multidisciplinary Optimization manuscript No.
(will be inserted by the editor)

H. Antil · R.H.W. Hoppe · C. Linsenmann

Optimal design of stationary flow problems by path-following interior-point methods

Received: date / Revised: date

Abstract We consider the numerical solution of structural optimization problems in CFD where the state variables are supposed to satisfy a linear or nonlinear Stokes system and the design variables are subject to bilateral pointwise constraints. Within a primal-dual setting, we suggest an all-at-once approach based on interior-point methods. The discretization is taken care of by Taylor-Hood elements with respect to a simplicial triangulation of the computational domain. The efficient numerical solution of the discretized problem relies on path-following techniques, namely a continuation method with an adaptive choice of the continuation step size and a long-step path-following algorithm. The performance of the suggested methods is documented by several illustrative numerical examples.

Keywords shape optimization, Stokes flow problems, path-following interior-point methods

1 Introduction

Optimal design problems associated with fluid flow problems play a decisive role in a wide variety of engineering applications (cf., e.g., Mohammadi and Pironneau (2001) and the references therein). A typical example is to design the geometry of the container of the fluid, e.g., a channel, a reservoir, or a network of channels and reservoirs, in such a way that a desired flow velocity and/or pressure profile is achieved. The solution of the problem amounts to the minimization of an objective functional that depends on the so-called state variables (velocity, pressure) and on the design variables which determine the geometry of the fluid filled domain. The state variables are supposed to satisfy the underlying fluid mechanical equations, and there are typically further technologically motivated constraints, e.g., bilateral constraints on the design variables which restrict the shape of the fluid filled domain to that what is technologically feasible.

Shape optimization problems have been extensively studied and are well documented in the literature (cf., e.g., the monographs Allaire (2002); Bendsoe (1995); Bendsoe and Sigmund (2003); Cherkaev (2000); Delfour and Zolesio (2001); Haslinger and Neittaanmäki (1988); Haslinger and Mäkinen (2004); Mohammadi and Pironneau (2001); Pironneau (1984); Rozvany (1989); Sokolowski and Zolesio (1992)). The traditional approach relies on a separate treatment of the design objective and the state equation by an iterative cycle that starts from a given design, computes an approximate solution of the state equation for that design, invokes some sensitivity analysis for an update of the design, and continues this way until convergence is achieved. In contrast to this successive approximation, recently so-called 'all-at-once methods' or 'one-shot methods' have attracted considerable attention in PDE constrained optimization whose characteristic feature is that the numerical solution of the state equation is an integral part of the optimization routine. In particular, it has been shown that this novel approach may lead to significant savings of computational time (see e.g. Biros and Ghattas (2005a,b); Böhm et al (2003); Hoppe et al (2006); Hoppe and Petrova (2004); Hoppe et al (2002); Shenoy et al (1998)).

In this paper, we consider the optimal design of stationary fluid flow problems as described by the Stokes

The first author acknowledges support by the Texas Learning and Computation Center TLC^2. The second and third authors acknowledge support by the NSF under Grant No. DMS-0411403 and Grant No. DMS-0511611 as well as by the DFG within the Priority Program SPP 1253'PDE Constrained Optimization'.

all authors
Department of Mathematics, University of Houston, Houston, TX 77204, USA
Tel.: +1-713-743-3452
Fax: +1-713-743-3505
E-mail: harbir@math.uh.edu E-mail: rohop@math.uh.edu E-mail: linsen@math.uh.edu

R.H.W. Hoppe, C. Linsenmann
Institute of Mathematics, University of Augsburg, D-86159 Augsburg, Germany
E-mail: hoppe@math.uni-augsburg.de

system. The objective is to design the geometry of a channel or a particular geometric feature of a channel such that a desired profile of the velocity and/or the pressure is realized as closely as possible. The design variables are chosen as the Bézier control points of a globally continuous Bézier curve representation of the walls of the channel. The control points are subject to bilateral constraints. For instance, for the shape optimization of a backward facing step (cf. Fig. 1), we have used a moderate number m_1 of control points for the upper wall and $m_2 \gg m_1$ control points for the lower wall including the backward facing step.
The approach that we are pursuing here is an 'all-at-once method' based on a primal-dual formulation where the Stokes system is coupled by Lagrange multipliers and the constraints on the design variables are taken care of by parameterized logarithmic barrier functions.

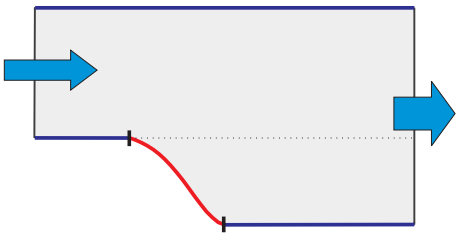

Fig. 1 Channel with a backward facing step

This leads to a family of minimization subproblems parameterized by the barrier parameter. The optimality conditions result in a parameter dependent nonlinear system whose solution gives rise to the so-called central path (cf., e.g., Forsgren et al (2002); Wright (1992)). A significant challenge is to follow the central path as closely as possible as the barrier parameter goes to zero. Here, we use two path-following strategies. The first one is an adaptive continuation method with tangent continuation as a predictor and Newton's method as a corrector following the ideas from Deuflhard (2004), whereas the second one is a variant of the long-step target following algorithm known from linear programming (cf., e.g., Wright (1997)). We note that path-following algorithms for shape optimization problems in structural mechanics have been used in Herskovits et al. (2000).

2 The shape optimization problem

We consider Stokes flow in a bounded domain $\Omega(\alpha) \subset \mathbb{R}^2$ with boundary $\Gamma(\alpha) = \Gamma_{in}(\alpha) \cup \Gamma_{lat}(\alpha) \cup \Gamma_{out}(\alpha)$, depending on the design variables $\alpha = (\alpha_1, \cdots, \alpha_m)^T \in \mathbb{R}^m$ which are chosen as the Bézier control points of a Bézier curve representation of the lateral boundaries of the domain. Denoting the viscosity of the fluid by ν, the velocity by $\mathbf{u}$ and the pressure by p, we refer to

$$J(\mathbf{u}, p, \alpha) := \frac{\kappa_1}{2} \int\limits_{\Omega(\alpha)} |\mathbf{u} - \mathbf{u^d}|^2 \, dx + \frac{\kappa_2}{2} \int\limits_{\Omega(\alpha)} |p - p^D|^2 \, dx$$

as the objective functional, where $\mathbf{u^d}, p^d$ are desired velocity and pressure profiles, and $\kappa_\nu, 1 \le \nu \le 2$, are appropriately chosen weighting factors. The shape optimization problem reads

$$\text{minimize } J(\mathbf{u}, p, \alpha) \tag{1}$$

subject to the Stokes system (state equations)

$$\begin{aligned} -\nabla \cdot \boldsymbol{\sigma}(\mathbf{u}) &= 0 \quad \text{in } \Omega(\alpha), && \text{(2a)} \\ \nabla \cdot \mathbf{u} &= 0 \quad \text{in } \Omega(\alpha), \\ \boldsymbol{\sigma}(\mathbf{u}) &= -p\mathbf{I} + g(\mathbf{u}, \mathbf{D}(\mathbf{u}))\mathbf{D}(\mathbf{u}), && \text{(2b)} \end{aligned}$$

with given boundary conditions on $\Gamma(\alpha)$ and subject to the bilateral constraints

$$\alpha_i^{min} \le \alpha_i \le \alpha_i^{max}, \ 1 \le i \le m. \tag{3}$$

on the design variables.
We note that in the constitutive equation (2b) the tensor $\mathbf{D}(\mathbf{u})$ stands for the rate of deformation tensor $\mathbf{D}(\mathbf{u}) := (\nabla\mathbf{u} + (\nabla\mathbf{u})^T)/2$ and $g(\mathbf{u}, \mathbf{D}(\mathbf{u}))$ denotes the viscosity function which is given by $g(\mathbf{u}, \mathbf{D}(\mathbf{u})) = \nu$ for linear Stokes flow and depends nonlinearly on $\mathbf{u}, \mathbf{D}(\mathbf{u})$ in the nonlinear regime.

For the finite element approximation of (1)-(3) we choose $\hat{\alpha} \in K$ as a reference design and refer to $\hat{\Omega} := \Omega(\hat{\alpha})$ as the associated reference domain. Then, the actual domain $\Omega(\alpha)$ can be obtained from the reference domain $\hat{\Omega}$ by means of a mapping $\Omega(\alpha) = \Phi(\hat{\Omega}; \alpha)$. The advantage of using the reference domain $\hat{\Omega}$ is that finite element approximations can be performed with respect to that fixed domain without being forced to remesh for every new set of the design variables.
For the discretization of the velocity $\mathbf{u}$ and the pressure p, we use Taylor-Hood P2/P1 elements (see e.g. Brezzi and Fortin (1991)) with respect to a shape regular family of simplicial triangulations of $\hat{\Omega}$ (Fig. 2 displays the finite element mesh for the final design of the channel with a backward facing step).

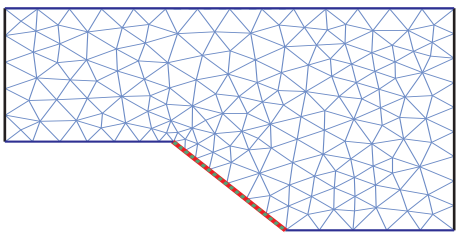

Fig. 2 Finite element mesh for the optimal design of a channel with a backward facing step

We denote by $\mathbf{u}_h \in \mathbb{R}^{n_1}$ and $p_h \in \mathbb{R}^{n_2}$ the vectors standing for the velocity components and the pressure in the nodal points associated with the Taylor-Hood finite element approximation of the Stokes system, and we refer to $J_h(\mathbf{u}_h, p_h, \alpha)$ as the discretized objective functional. Then, the discrete optimal design problem can be stated as follows:

$$\text{minimize } J_h(\mathbf{u}_h, p_h, \alpha) \tag{4}$$

subject to the algebraic system (discretized Stokes equations)

$$S_h(\alpha)\mathbf{y}_h \;:=\; \begin{pmatrix} A_h(\mathbf{u}_h,\alpha) & B_h^T(\alpha) \\ B_h(\alpha) & 0 \end{pmatrix} \begin{pmatrix} \mathbf{u}_h \\ p_h \end{pmatrix} = \mathbf{g}_h, \tag{5}$$

where $\mathbf{y}_h := (\mathbf{u}_h, p_h)^T$ and $A_h(\mathbf{u}_h, \alpha) : \mathbb{R}^{n_1} \times \mathbb{R}^m \to \mathbb{R}^{n_1}$, $B_h(\alpha) \in \mathbb{R}^{n_2 \times n_1}$, and further subject to the inequality constraints

$$\alpha_i^{min} \;\le\; \alpha_i \;\le\; \alpha_i^{max}\;,\; 1 \le i \le m. \tag{6}$$

Due to the highly nonlinear dependence on the design variables, (4)-(6) represents an inequality constrained nonlinear programming problem. It will be numerically solved by path-following primal-dual interior-point methods as described in the next section. For ease of notation, in the sequel we will drop the subindex h.

3 Path-following interior-point methods

We couple the inequality constraints (3) by logarithmic barrier functions with a barrier parameter $\beta = 1/\mu > 0$, $\mu \to \infty$, and the the PDE constraint (2) by a Lagrange multiplier $\boldsymbol{\lambda} = (\boldsymbol{\lambda}_\mathbf{u}, \lambda_p)^T$. This leads to the saddle point problem

$$\inf_{\mathbf{y},\alpha} \sup_{\boldsymbol{\lambda}} L^{(\mu)}(\mathbf{y}, \boldsymbol{\lambda}, \alpha)\;, \tag{7}$$

where $L^{(\mu)}$ stands for the Lagrangian

$$L^{(\mu)}(\mathbf{y}, \boldsymbol{\lambda}, \alpha) \;=\; B^{(\mu)}(\mathbf{y}, \alpha) \;+\; \langle S(\mathbf{y}, \alpha) - \mathbf{g}, \boldsymbol{\lambda} \rangle\;, \tag{8}$$

and $B^{(\mu)}(\mathbf{y}, \alpha)$ is the so-called barrier function as given by

$$B^{(\mu)}(\mathbf{y}, \alpha) \;:= \tag{9}$$
$$J(\mathbf{y}, \alpha) \;-\; \frac{1}{\mu} \sum_{i=1}^{m} [\ln(\alpha_i - \alpha_i^{\min}) + \ln(\alpha_i^{\max} - \alpha_i)]\;.$$

It is well-known (cf., e.g., Wright (1992)) that for sufficiently large μ the minimization subproblems

$$\inf_{\mathbf{y},\alpha} B^{(\mu)}(\mathbf{y}, \alpha) \tag{10}$$

admit unique local minima which converge to a strict local minimum of (4)-(6) as $\mu \to \infty$.

The central path $\mu \longmapsto x(\mu) := (\mathbf{y}(\mu), \boldsymbol{\lambda}(\mu), \alpha(\mu))^T$ is given as the solution of the nonlinear system

$$F(x(\mu), \mu) \;=\; \begin{pmatrix} L_\mathbf{y}^{(\mu)}(\mathbf{y}, \boldsymbol{\lambda}, \alpha) \\ L_{\boldsymbol{\lambda}}^{(\mu)}(\mathbf{y}, \boldsymbol{\lambda}, \alpha) \\ L_\alpha^{(\mu)}(\mathbf{y}, \boldsymbol{\lambda}, \alpha) \end{pmatrix} \;=\; 0\;, \tag{11}$$

where the subindices refer to the derivatives of the Lagrangian with respect to the primal, the dual, and the design variables.
We consider the solution of (11) by an adaptive continuation method and a variant of the long-step path-following method.

3.1 Adaptive continuation method

The adaptive continuation method is a predictor-corrector method with an adaptively determined continuation step size in the predictor and Newton's method as a corrector (cf., e.g., Deuflhard (2004)).

Predictor Step: The predictor step relies on tangent continuation along the trajectory of the Davidenko equation

$$F_\mathbf{x}(\mathbf{x}(\mu), \mu)\; \mathbf{x}'(\mu) \;=\; -F_\mu(\mathbf{x}(\mu), \mu)\;. \tag{12}$$

Given some approximation $\tilde{\mathbf{x}}(\mu_k)$ at $\mu_k > 0$, compute $\tilde{\mathbf{x}}^{(0)}(\mu_{k+1})$, where $\mu_{k+1} = \mu_k + \Delta\mu_k^{(0)}$, according to

$$F_x(\tilde{\mathbf{x}}(\mu_k), \mu_k)\; \delta\mathbf{x}(\mu_k) \;=\; -\; F_\mu(\tilde{\mathbf{x}}(\mu_k), \mu_k)\;, \tag{13a}$$
$$\tilde{\mathbf{x}}^{(0)}(\mu_{k+1}) \;=\; \tilde{\mathbf{x}}(\mu_k) \;+\; \Delta\mu_k^{(0)}\; \delta\mathbf{x}(\mu_k)\;. \tag{13b}$$

We use $\Delta\mu_0^{(0)} = \Delta\mu_0$ for some given initial step size $\Delta\mu_0$, whereas for $k \ge 1$ the predicted step size $\Delta\mu_k^{(0)}$ is chosen by

$$\Delta\mu_k^{(0)} \;:= \tag{14}$$
$$\Big(\frac{\|\Delta\mathbf{x}^{(0)}(\mu_k)\|}{\|\tilde{\mathbf{x}}(\mu_k) - \tilde{\mathbf{x}}^{(0)}(\mu_k)\|}\; \frac{\sqrt{2}-1}{2\Theta(\mu_k)}\Big)^{1/2}\; \Delta\mu_{k-1}\;,$$

where $\Delta\mu_{k-1}$ is the computed continuation step size, $\Delta\mathbf{x}^{(0)}(\mu_k)$ is the first Newton correction (see below), and $\Theta(\mu_k) < 1$ is the contraction factor associated with a successful previous continuation step.

Corrector step: As a corrector, we use Newton's method applied to $F(\mathbf{x}(\mu_{k+1}), \mu_{k+1}) = 0$ with $\tilde{\mathbf{x}}^{(0)}(\mu_{k+1})$ from (13) as a start vector. In particular, for $\ell \ge 0$ and $j_\ell \ge 0$ we compute $\Delta x^{(j_\ell)}(\mu_{k+1})$ according to

$$F'(\tilde{x}^{(j_\ell)}(\mu_{k+1}), \mu_{k+1})\; \Delta x^{(j_\ell)}(\mu_{k+1}) \;= \tag{15}$$
$$-\; F(\tilde{x}^{(j_\ell)}(\mu_{k+1}), \mu_{k+1})$$

and $\overline{\Delta x}^{(j_\ell)}(\mu_{k+1})$ as the associated simplified Newton correction

$$F'(\tilde{x}^{(j_\ell)}(\mu_{k+1}), \mu_{k+1})\; \overline{\Delta x}^{(j_\ell)}(\mu_{k+1}) \;= \tag{16}$$
$$-\; F(\tilde{x}^{(j_\ell)}(\mu_{k+1}) + \Delta x^{(j_\ell)}(\mu_{k+1}), \mu_{k+1})\;.$$

We monitor convergence of Newton's method by means of

$$\Theta^{(j_\ell)}(\mu_{k+1}) \;:=\; \|\overline{\Delta x}^{(j_\ell)}(\mu_{k+1})\|/\|\Delta x^{(j_\ell)}(\mu_{k+1})\| \;.$$

In case of successful convergence, we accept the current step size and proceed with the next continuation step. However, if the monotonicity test

$$\Theta^{(j_\ell)}(\mu_{k+1}) \;<\; 1 \tag{17}$$

fails for some $j_\ell \geq 0$, the continuation step has to be repeated with the reduced step size

$$\begin{aligned} \Delta\mu_k^{(\ell+1)} &:= \Big(\frac{\sqrt{2}-1}{g(\Theta^{(j_\ell)})}\Big)^{1/2}\,\Delta\mu_k^{(\ell)} \;, \\ g(\Theta) &:= \sqrt{\Theta+1}-1 \end{aligned} \tag{18}$$

until we either achieve convergence or for some prespecified lower bound $\Delta\mu_{min}$ observe

$$\Delta\mu_k^{(\ell+1)} \;<\; \Delta\mu_{min} \;.$$

In the latter case, we stop the algorithm and report convergence failure.
The Newton steps are realized by an inexact Newton method featuring right-transforming iterations (cf., e.g., Hoppe et al (2006); Hoppe and Petrova (2004)). The derivatives occurring in the KKT conditions and the Hessians are computed by automatic differentiation (cf., e.g., Griewank (2000)).

3.2 Long-step path-following method

The long-step path-following method is based on the slack variable formulation of the KKT system with respect to the slack variables $\mathbf{z} = (z_1, z_2)^T$ with

$$\begin{aligned} z_{1,i} &:= \frac{\sigma}{\mu\;(\alpha_i - \alpha_i^{\min})} \;, \\ z_{2,1} &:= \frac{\sigma}{\mu\;(\alpha_i^{\max} - \alpha_i)} \quad , \quad 1 \leq i \leq m \;, \end{aligned} \tag{19}$$

where $\sigma > 0$ stands for the centering parameter.
A Newton step in the increments

$$\Delta x \;:=\; (\Delta\mathbf{y}, \Delta\boldsymbol{\lambda}, \Delta\alpha, \Delta\mathbf{z})^T$$

reads as follows (for notational convenience, in the following the upper index (μ) in the Lagrangian will be dropped):

$$\begin{pmatrix} I_\kappa(\alpha) & \boldsymbol{\nabla} S(\alpha) & L_{\mathbf{y},\alpha} & 0 \\ \boldsymbol{\nabla} S(\alpha) & 0 & L_{\boldsymbol{\lambda},\alpha} & 0 \\ L_{\alpha,\mathbf{y}} & L_{\alpha,\boldsymbol{\lambda}} & L_{\alpha,\alpha} & \hat{I} \\ 0 & 0 & \hat{Z} & D \end{pmatrix} \begin{pmatrix} \Delta\mathbf{y} \\ \Delta\boldsymbol{\lambda} \\ \Delta\alpha \\ \Delta\mathbf{z} \end{pmatrix} \;=\; -\tilde{\mathbf{g}} \;. \tag{20}$$

Here, $L_{\mathbf{y},\alpha}$ etc. stand for the second derivatives of the Lagrangian and

$$\begin{aligned} &I_\kappa(\alpha) := \mathrm{diag}(\kappa_1 I_1(\alpha), \kappa_2 I_2(\alpha)) \;,\; \hat{I} := (-I, I) \;, \\ &\hat{Z} := (Z_1, -Z_2)^T \;,\; D := \mathrm{diag}(D_1, D_2) \;, \\ &\tilde{\mathbf{g}} := (\mathbf{g}, D_1 Z_1 e - \sigma\mu^{-1} e, D_2 Z_2 e - \sigma\mu^{-1} e)^T \;, \end{aligned}$$

where $Z_1 := \mathrm{diag}(z_{1,i}), Z_2 := \mathrm{diag}(z_{2,i}), D_1 := \mathrm{diag}(\alpha_i - \alpha_i^{min}), D_2 := \mathrm{diag}(\alpha_i^{max} - \alpha_i)$, and $e := (1, 1, \cdots, 1)^T$.
We define $\mathcal{N}_{-\infty}(\gamma), 0 < \gamma \ll 1$, as the following neighborhood of the central path

$$\mathcal{N}_{-\infty}(\gamma) := \{(\mathbf{y}, \boldsymbol{\lambda}, \alpha, \mathbf{z}) \mid \mathbf{s}_\alpha^T \mathbf{z} \geq \mu^{-1}\gamma\} \;, \tag{21}$$

where $\mathbf{s}(\alpha) := (s_1(\alpha), s_2(\alpha))^T, s_1(\alpha) := \alpha - \alpha^{min}, s_2(\alpha) := \alpha^{max} - \alpha$.
The long-step path-following algorithm proceeds as follows:

Initialization: Specify $0 < \gamma \ll 1$, bounds $0 < \sigma_{min} < \sigma_{max} < 1$ for the centering parameter, and choose a start iterate

$$\mathbf{x}^{(0)} = (\mathbf{y}^{(0)}, \boldsymbol{\lambda}^{(0)}, \alpha^{(0)}, \mathbf{z}^{(0)}) \in \mathcal{N}_{-\infty}(\gamma) \;.$$

Iteration loop: For $k = 0, 1, 2, \cdots$ set

$$\mu^{(k)} := \max\Big(\frac{m}{(s_1^{(k)})^T z_1^{(k)}}, \frac{m}{(s_2^{(k)})^T z_2^{(k)}}\Big)$$

where $s_\nu^{(k)} := s_\nu(\alpha^{(k)}, 1 \leq \nu \leq 2$.
Choose $\sigma_k \in (\sigma_{min}, \sigma_{max})$, and compute

$$\Delta\mathbf{x}^{(k)} = (\Delta\mathbf{y}^{(k)}, \Delta\boldsymbol{\lambda}^{(k)}, \Delta\alpha^{(k)}, \Delta\mathbf{z}^{(k)})$$

as the solution of (20). Set

$$\begin{aligned} \mathbf{x}^{(k+1)} &:= \mathbf{x}^{(k)} + \eta_k \Delta\mathbf{x}^{(k)} \;, \\ \eta_k &:= \max\{\eta \in (0,1) \mid \mathbf{x}^{(k)} + \eta\Delta\mathbf{x}^{(k)} \in \mathcal{N}_{-\infty}(\gamma)\} \;. \end{aligned}$$

Given a tolerance *tol*, the iteration will be terminated, if $J(\mathbf{y}^{(k)}, \alpha^{(k)}) < tol$. For $k \geq 1$, a possible choice of the centering parameter $\sigma^{(k)}$ is $\sigma^{(k)} := \Big(\mu^{(k-1)}/\mu^{(k)}\Big)^2$.
The solution of (20) is computed based on static condensation of the slack variables and the application of right-transforming iterations to the resulting reduced Hessian system (cf., e.g., Hoppe et al (2006); Hoppe and Petrova (2004)) using automatic differentiation for the computation of the derivatives (cf., e.g., Griewank (2000)).

4 Applications

4.1 Channel with a backward facing step

As a benchmark problem, we consider linear Stokes flow in a channel with a backward facing step (cf. Figure 1). The initial shape (straight line) and the optimal shape

(dotted line) with regard to a desired velocity field according to prespecified design $\bar{\alpha}$ are shown in 3. Here, the three horizontal segments of the geometry are fixed and only the segment that connects the two lower horizontal segments is variable. In this setting, the function that describes the bottom segment of the geometry is a composite Bézier curve consisting of three curves of degree 0, 4 and 0, respectively. Note that the composite curve is only continuous. The data for this geometry is as follows

$$\hat{\Omega} = \Omega(\alpha^0), \alpha^0 = (+1.0, -0.5, -0.5, -1.5, -1.5, -1.5)^T,$$
$$\bar{\alpha} = (+1.0, -0.5, -0.55, -0.6, -0.6, -1.5)^T,$$
$$\nu = 1.0\ ,\ u_{in}(x_1, x_2) = (6(1+x_2)(1-x_2),\ 0),$$
$$\alpha^{min} = (0, -5, -5, -5, -5, -5)^T,$$
$$\alpha^{max} = (5, 0, 0, 0, 0, 0)^T.$$

The problem has been solved using the adaptive continuation method as described in subsection 3.1. Table 4.1 reflects the convergence history of the iterative process. Here, the columns labeled J and Θ contain the actual values of the objective functional and the contraction factor in the monotonicity test, respectively. Repeated occurrence of the iteration counter k means that a correction step had to be performed with a reduced continuation step size due to a failure of the monotonicity test.
Figure 4 displays the velocity field (top) and the pressure distribution (bottom) for the computed optimal shape.

Table 1 Convergence history of the continuation method

k	μ	$\Delta\mu$	J	Θ
0	100.0	300.0	2.6e+00	–
1	100.0	300.0	9.6e-01	0.58
			1.3e-01	618.42
1	100.0	425.5	4.3e-04	0.11
2	525.5	417.1	2.3e-03	0.41
			2.3e-03	0.58
			2.0e-03	0.92
			1.6e-05	0.43
			2.5e-05	–
3	942.6	323.5	5.1e-05	0.34
4	1266.1	283.7	4.9e-05	0.27
5	1549.8	593.1	3.3e-05	0.05
6	2142.9	2265.3	1.7e-05	0.01
7	4408.2	–	1.9e-07	–

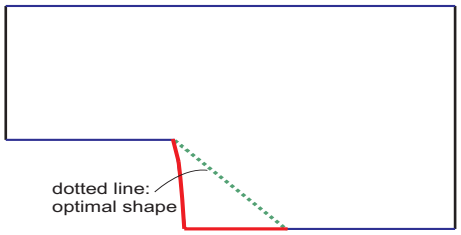

Fig. 3 Initial and optimal shape of the backward facing step.

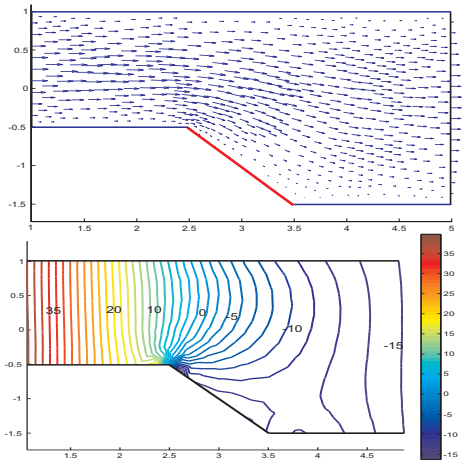

Fig. 4 Velocity field (top) and pressure distribution (bottom) associated with the optimal shape.

4.2 Capillary barrier

Programmable microfluidic biochips and microarrays are used in pharmaceutical, medical and forensic applications as well as in academic research and development for high throughput screening, genotyping and sequencing by hybridization in genomics, protein profiling in proteomics, and cytometry in cell analysis). They are miniaturized biochemical labs that are physically and/or electronically controllable and guarantee a precise positioning of the samples (e.g., DNA solutes or proteins) on the surface of the chip. Recent technology uses Surface Acoustic Wave (SAW) driven microfluidic biochips whose operating principle is based on piezoelectrically actuated surface acoustic waves on the surface of a chip which transport the droplet containing probe along a lithographically produced network to reservoirs at prespecified surface locations serving as miniaturized chemical labs. They allow the in-situ investigation of the dynamics of hybridization processes with extremely high time resolution (see e.g. Pollard and Castrodale (2003); Wagner et al (2002); Wixforth et al (2002)). Figure 5 gives an illustration of such a microfluidic biochip.

One of the issues in the optimal design of the biochips is to make sure that the reservoir is filled with a very precise amount of the probe containing liquid. This is taken care of by a capillary barrier placed between a channel and the reservoir (see Fig. 6).
The SAW induced fluid flow in the channels can be described by a multiphysics and multi-scale system consisting of the linearized equations of piezoelectricity coupled with the compressible Navier-Stokes equations. The induced fluid flow involves on very different time scales. The SAWs enter the fluid filled channels within nanoseconds creating sharp jets in the fluid which get signifi-

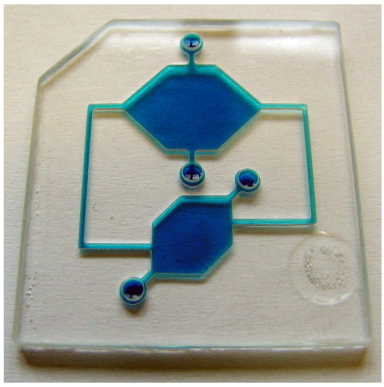

Fig. 5 Surface Acoustic Wave (SAW) driven microfluidic biochip

cantly damped while propagating along the channels. After a couple of milliseconds, a stationary flow pattern is formed, called acoustic streaming, which describes the transport of the probes within the network. Since the acoustic streaming can be modeled by stationary Stokes flow obtained by the application of appropriate homogenization techniques, the optimal design of the capillary barriers fits the framework set in this paper. We refer to Antil et al (2007); Gantner et al (2007); Köster (2007) for details.

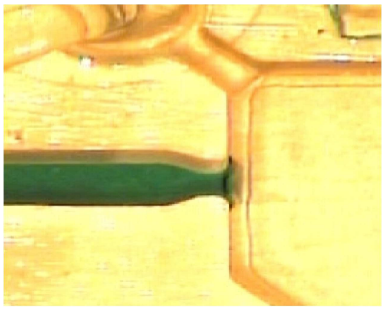

Fig. 6 Channel with capillary barrier on an SAW driven microfluidic biochip

As computational domain we have chosen a channel with a capillary barrier at its end and part of a reservoir connected with the channel by the capillary barrier. The problem has been discretized by Taylor-Hood elements and we have applied the long-step path-following method from subsection 3.2 using a Bézier curve representation of the barrier. Figure 7 displays the computed optimal shape of the barrier with respect to a prespecified velocity field and pressure distribution together with an underlying finite element mesh. The channel additionally has passive outlet valves (cf. Figure 7) that are activated when the barrier operates in stopping mode and back flow occurs.

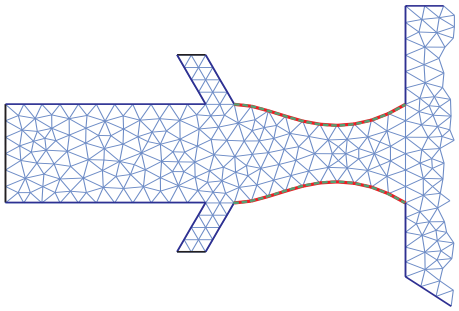

Fig. 7 Optimal shape of the capillary barrier and underlying finite element mesh

Figure 8 provides a visualization of the velocity field for the optimized channel under conditions of flow from the channel into the reservoir.

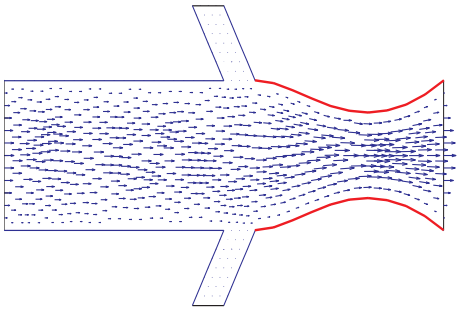

Fig. 8 Velocity field for the optimal configuration when the barrier is not in stopping mode

Likewise, Figure 9 displays the velocity field for the optimized channel under back flow conditions, i.e., when the capillary barrier operates in stopping mode.

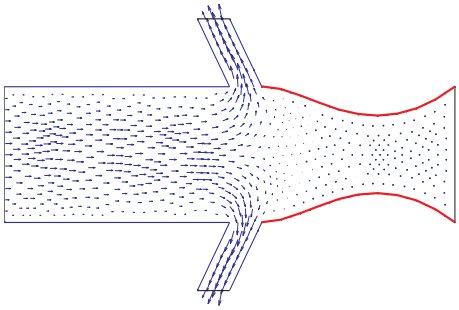

Fig. 9 Velocity field (back flow) for the optimal configuration when the barrier is in stopping mode

4.3 Electrorheological shock absorbers

Electrorheological shock absorbers are based on electrorheological fluids (ERF) which are suspensions of small electrically polarizable particles dissolved in nonconducting

liquids such as silicon oils. Under the influence of an outer electric field the particles form chains along the electric field lines and then aggregate to form larger and larger columns thus changing the viscosity of the fluid. This is called the electrorheological effect which happens within a few milliseconds and is reversible. Due to the electrorheological effect, ERF are used in all technological processes where a controlled power transmission plays a significant role such as automotive shock absorbers (see Filisko (1995)). Figure 10 (left) gives a schematic representation of an ERF absorber which consists of two fluid chambers connected by small ducts within the piston. The walls of the ducts serve as the electrodes, and the power supply is guaranteed by an external source connected to the electrodes through the piston rod.

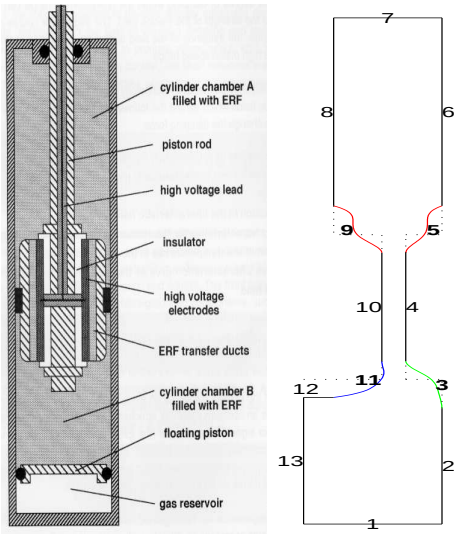

Fig. 10 Electrorheological shock absorber: schematic diagram (left) and Bézier curve representation of the inlet and outlet boundaries of the right part of the fluid chamber (right)

An important optimization issue is to design the inflow and outflow boundaries of the ducts both in the compression mode (piston is moving down) and in the rebound mode (piston is moving up) such that pressure peaks are avoided which may cause inappropriate damping profiles. This amounts to the solution of a pressure tracking problem where the state equations are given by the stationary ERF equations

$$-\nabla\cdot\boldsymbol{\sigma}(\mathbf{u}) = \mathbf{f} \quad \text{in } \Omega(\alpha)\ , \tag{22}$$

$$\nabla\cdot\mathbf{u} = 0 \quad \text{in } \Omega(\alpha) \tag{23}$$

along with appropriate boundary conditions. Here, $\mathbf{u} = (u_1, u_2)$ is the velocity vector, $\boldsymbol{\sigma}$ refers to the stress tensor and $\mathbf{f}$ describes exterior forces acting on the fluid. The stress tensor $\boldsymbol{\sigma}$ is related to the rate of deformation tensor $(\mathbf{D}(\mathbf{u}))_{ij} := (\partial u_i/\partial x_j + \partial u_j/\partial x_i)/2\ ,\ 1 \le i,j \le 2$, by a constitutive equation where the electric field $\mathbf{E}$ enters as a parameter

$$\boldsymbol{\sigma} \;=\; -p\,\mathbf{I} \;+ 2\,\varphi(I(\mathbf{u}), |\mathbf{E}|, \mu(\mathbf{u},\mathbf{E}))\,\mathbf{D}(\mathbf{u})\ . \tag{24}$$

Note that φ is a viscosity function depending on the shear rate $I(\mathbf{u})$, the electric field strength $|\mathbf{E}|$, and the angle $\mu(\mathbf{u},\mathbf{E})$ between the velocity field $\mathbf{u}$ and the electric field $\mathbf{E}$. We refer to Hoppe and Litvinov (2004); Hoppe et al (2003) for details.
A computed optimal shape of the outlet boundary in the rebound mode based on the continuation method from subsection 3.1 is shown in Figure 11 (right). For details we refer to Hoppe et al (2006).

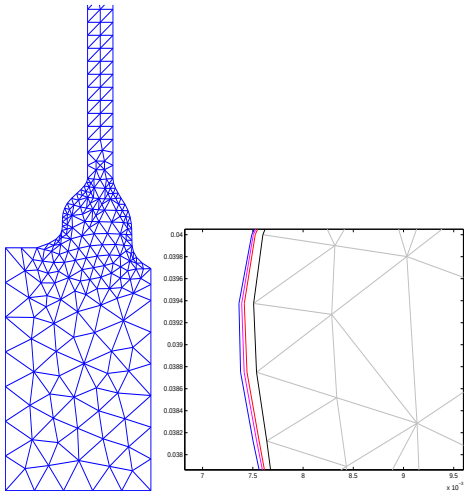

Fig. 11 Optimized outlet boundary (left) and details of the optimal design for various electric field strengths (right)

5 Conclusions

We have provided an 'all-at-once approach' for the optimal design of stationary flow problems described by linear and nonlinear Stokes flow featuring path-following primal-dual interior-point methods by means of an adaptive predictor-corrector type continuation method and a long-step path-following algorithm. The computation of the first order derivatives in the KKT systems and the second order derivatives in the Hessians is significantly facilitated by automatic differentiation. Numerical examples including a benchmark problem and two real-life design problems demonstrate that both methods can be efficiently used in shape optimization.

References

Allaire G (2002) Shape Optimization by the Homogenization Method. Springer, Berlin-Heidelberg-New York.

Antil H, A. Gantner A, Hoppe, R H W, Köster D, Siebert K G, and Wixforth A (2007) Modeling and Simulation of Piezoelectrically Agitated Acoustic Streaming on Microfluidic Biochips. submitted to Proc. 17th Int. Conf. on Domain Decomposition Methods.

Bendsøe M P (1995) Optimization of Structural Topology, Shape, and Material. Springer, Berlin-Heidelberg-New York.

Bendsøe M P, and Sigmund O (2003) Topology Optimization: Theory, Methods and Applications. Springer, Berlin-Heidelberg-New York.

Biros G, and Ghattas O (2005) Parallel Lagrange-Newton-Krylov-Schur methods for PDE-constrained optimization. part i: the Krylov-Schur solver. SIAM J. Sci. Comp. 27, 687–713.

Biros G, and Ghattas O (2005) Parallel Lagrange-Newton-Krylov-Schur methods for PDE-constrained optimization. part ii: the Lagrange-Newton solver and its application to optimal control of staedy viscous flows. SIAM J. Sci. Comp. 27, 714–739.

Böhm P, Hoppe R H W, Mazurkevitch G, Petrova S I, Wachutka G, and Wolfgang E (2003) Optimal structural design of high power electronic devices by topology optimization. In: Mathematics - Key Technology for the Future. Cooperations between Mathematics and Industry (Krebs H, and Jäger W (eds.)), pp. 365–376, Springer, Berlin-Heidelberg-New York.

Cherkaev A (2000) Variational Methods for Structural Optimization. Springer, New York.

Brezzi F, and Fortin, M (1991) Mixed and Hybrid Finite Element Methods. Springer, Berlin-Heidelberg-New York.

Byrd, R H, Hribar M E, and Nocedal, J (1999) An interior point algorithm for large scale nonlinear programming. SIAM J. Optimization 9, 877–900.

Delfour M C, and Zolesio J P (2001) Shapes and Geometries: Analysis, Differential Calculus and Optimization. SIAM, Philadelphia.

Deuflhard P (2004) Newton Methods for Nonlinear Problems. Affine Invariance and Adaptive Algorithms. Springer, Berlin-Heidleberg-New York.

Filisko F (1995) Overview of ER technology. In: Progress in ER technology (Havelka K (ed.)), Plenum Press, New York.

Forsgren A, Gill Ph E, and Wright M H (2002) Interior methods for nonlinear optimization. SIAM Rev. 44, 522–597.

Gantner A, Hoppe R H W, Köster D, Siebert K G, and Wixforth A (2007) Numerical simulation of piezoelectrically agitated surface acoustic waves on microfluidic biochips. Comp. Visual. Sci. DOI 10.1007/5 00791-006-0040-y (in press)

Griewank A (2000) Evaluating Derivatives, Principles and Techniques of Automatic Differentiation. SIAM, Phildelphia.

Haslinger J, and Neittaanmäki P (1988) Finite Element Approximation for Optimal Shape Design: Theory and Applications. John Wiley & Sons, Chichester.

Haslinger J, and Mäkinen R A E (2004) Introduction to Shape Optimization: Theory, Approximation, and Computation. SIAM, Philadelphia.

Herskovits J, Dias G, Santos G, and Mota Soares C M (2000) Shape structural optimization with an interior point nonlinear programming algorithm. Struct. Multidisc. Optim. 20, 107–115.

Hoppe R H W, Linsenmann C, and Petrova S I (2006) Primal-dual Newton methods in structural optimization. Comp. Visual. Sci. 9, 71–87.

Hoppe R H W, and Litvinov W G (2004) Problems on electrorheological fluid flows. Communications in Pure and Applied Analysis 3, 809–848.

Hoppe R H W, Litvinov W G, and T. Rahman T (2003) Mathematical modeling and numerical simulation of electrorheological devices and systems. In: Proc. Int. Conf. on Scientific Computing, Jyväskylä, Finland, June 14/15, 2002 (Neittaanmäki P, and Pironneau O (eds.)), pp. 80–93, CIMNE, Barcelona.

Hoppe R H W, and Petrova S I (2004) Primal-dual Newton interior-point methods in shape and topology optimization. Numer. Linear Algebra Appl. 11, 413–429.

Hoppe R H W, Petrova S I, and V. Schulz V (2002) A primal-dual Newton-type interior-point method for topology optimization. Journal of Optimization: Theory and Applications 114, 545-571.

Köster D (2007) Numerical simulation of acoustic streaming on SAW-driven biochips. submitted to SIAM J. Comp. Sci.

Mohammadi B, and Pironneau O (2001) Applied Shape Optimization for Fluids. Oxford University Press, Oxford.

Pironneau O (1984) Optimal Shape Design for Elliptic Systems. Springer, Berlin-Heidelberg-New York.

Pollard J, and Castrodale B (2003) Outlook for DNA microarrays: emerging applications and insights on optimizing microarray studies. Report. Cambridge Health Institute, Cambridge.

Rozvany G (1989) Structural Design via Optimality Criteria. Kluwer, Dordrecht.

Shenoy A R, Heinkenschloss M, and Cliff E M (1998) Airfoil design by an all-at-once approach. Int. J. Comput. Fluid Mechanics 11, 3–25.

Sokolowski J, and Zolesio, J P (1992) Introduction to Shape Optimization. Springer, Berlin-Heidelberg-New York.

Wagner P, Tan M X, Zaugg F G, and Indermühle P F (2002) Protein biochips: protein analysis on a small scale. mst news 5, 44.

Wittum G (1989) On the convergence of multigrid iterations with transforming smoothers. Theory with applications to the Navier-Stokes equations. Numer. Math. 57, 15-38.

Wixforth A, Scriba J, and Gauer G (2002) Flatland fluidics. mst news 5, 42-43.

Wright M H (1992) Interior methods for constrained optimization. Acta Numerica 1, 341-407.

Wright S J (1997) Primal-Dual Interior-Point Methods. SIAM, Philadelphia.